AN EXTENDED ELECTRON BEAM FOR AURORAL STUDIES

by

Manuel Martinez-Sanchez
Department of Aeronautics and Astronautics, MIT
77 Massachusetts Ave, Cambridge, MA 02139
and
Juan R. Sanmartin
ETSI Aeronautics, Universidad Politecnica de Madrid
Madrid, 28040 SPAIN

Abstract

An electrically floating metallic bare tether in a low Earth orbit would be highly negative with respect to the ambient plasma over most of its length, and would be bombarded by ambient ions. This would liberate secondary electrons, which, after acceleration through the same voltage, would form a magnetically guided two-sided planar e-beam. Upon impact on the atmospheric E-layer, at about 120-140 Km altitude auroral effects (ionization and light emission) can be expected. This paper examines in a preliminary way the feasibility of using this effect as an upper atmospheric probe. It is concluded that significant perturbations can be produced along the illuminated planar sheet of the atmosphere, with ionization rates of several thousand cm^{-3} sec^{-1}. Observation of the induced optical emission is made difficult by the narrowness and high moving speed of the illuminated zone, but it is shown that vertical resolution of single spectral lines is possible, as is wider spectral coverage with no vertical resolution.

1. Introduction

The electrodynamic interaction of an orbiting conductive tether with the Earth's magnetic field and with the ionosphere has received attention for potential applications ranging from power generation and/or propulsion [1] to ELF wave generation. Various studies have identified as a bottleneck the efficient capture of ionospheric electrons at the anodic end of the tether, which has motivated theoretical and experimental work on plasma contactors [2], [3]. As a simple alternative, Ref. 5 has proposed the use of uninsulated metallic tethers, whose anodic end would collect electrons in an orbital motion limited regime with moderately small voltage drops. This anodic segment would extend roughly to the upper 1/7 of the tether length, for an upwards-deployed tether with a load and a cathodic contactor at its lower end. The remaining 6/7 of the tether would be at a negative potential relative to the local plasma (Fig. 1). If left bare, this portion of the tether would collect ions, countering to some extent the effect of the anodic

segment. However, for a voltage bias ΔV the ionic current collected per unit length scales as $\sqrt{\Delta V / m_i}$, and is therefore much smaller than the corresponding electronic current collected per unit length in the upper segment (scaling as $\sqrt{\Delta V / m_e}$). This justifies a fully bare tether design.

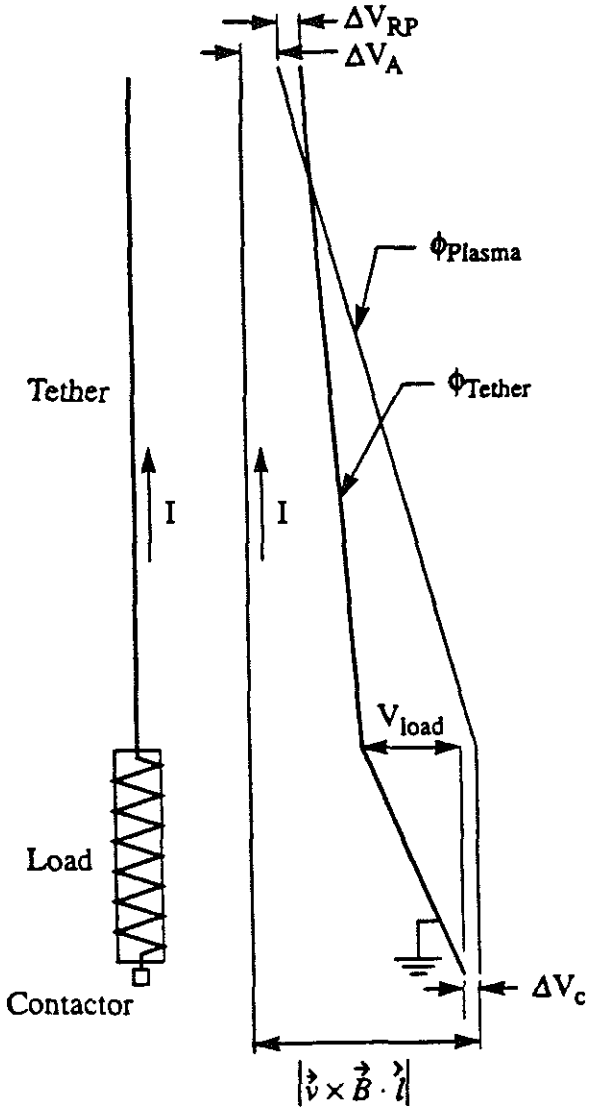

Fig. 1: Potential diagram for tether as a generator. Load at bottom, tether deployed upwards.

As Fig. 1 indicates, ions striking the metallic tether near its base would arrive with an energy of the order of the full induced emf vBL of the tether, i.e., some 2000-4000 V for a 20 Km long tether in a 28° LEO orbit. This bombarding energy decreases more or less linearly towards zero at the cross-

over point near the top. One of the consequences of this bombardment is the emission of secondary electrons. The yield γ (electrons/ion) is of the order of a few per cent at low energies, and increase about linearly with ion energy, to perhaps 20% at the 1 KV level. For a typical 20 Km long, 2mm diameter wire, secondary electron currents of the order of 60 mA can be expected. These electrons are accelerated by the tether-to-plasma local voltage, and are then channeled by the geomagnetic field, with a range of pitch angles, clustered about the value of the local magnetic dip angle. From this point, these electrons would constitute an e-beam racing down the magnetic lines much like those that are known to cause auroral displays at high latitudes.

Auroral studies [5],[6],[7], have always been hampered by the difficulty in obtaining precise information about the characteristics of the naturally precipitating electrons. Natural auroral events occur at random times and vary rapidly and irregularly in space and time, which makes in-situ observation with sounding rockets a chancy affair. Remote observation from overflying satellites has allowed very complete mapping of luminosities, but has yielded little correlating information on the energy, spectrum and pitch distribution of the originating electrons. Some active e-beam experiments have been carried out [8], [9], but the small transverse dimensions of the e-beam (typically of the order of 2x Larmor radius, or about 10 m) make detailed observation of the luminosity difficult.

By contrast, the large area illuminated by the tether-generated e-beam (~10 m $\times$ 20 Km) and its controllability by manipulation of the load and/or the end contactors, makes it a very appealing probe for auroral studies. Observation can be either from the spacecraft (allowing extended integration times) or from the ground (taking advantage of precise knowledge of the timing and location of the e-beam). The atmospheric layer probed is in the 120-140 Km range, which is difficult to access by other methods, and vertical resolution may be possible. With a well-defined electron flux, measurements of induced ionization and photo-emission rates and comparison to detailed simulations should provide a wealth of information on many kinetic rates which are at present only schematically known, and may uncover new aeronomic mechanisms of importance in the thermosphere.

In this paper we present a preliminary feasibility study for this concept. Section 2 reviews the geometric and electrodynamic aspects of the tether current generation. Section 3 presents a simplified model of the interaction of an electron beam with the upper atmosphere and gives estimates of the induced rates. Section 4 considers the observational options and their feasibility.

2. Tether Characteristics and Electron Emission

For this particular application, where we have no need for the tether as a generator, it is best to maximize the voltages available by deactivating the cathodic contactor at the bottom. Also, in order to reduce the high voltage exposure of the spacecraft, the tether should be deployed downwards. Fig. 2

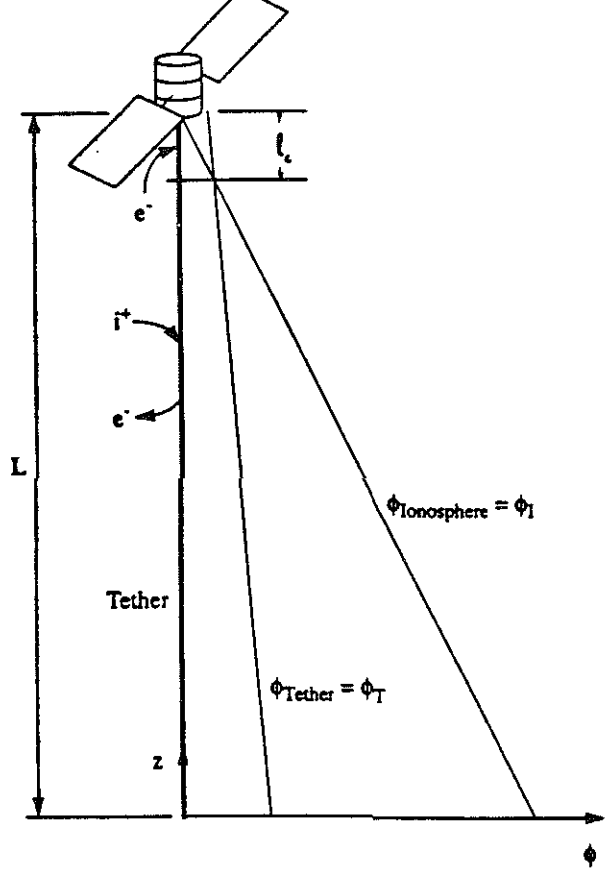

Fig. 2: Potential Diagram roughly

shows a schematic of the configuration. The ionospheric potential, in the vehicle's frame, decreases upwards at a rate

$$E = \left(\bar{v} \times \bar{B}\right)_z \qquad (1)$$

where $\bar{v}$ is the orbital velocity and $\bar{B}$ the geomagnetic field. The tether supports only the small levels of current due to ion collection, and will be regarded in a first approximation as being equipotential, floating at a positive potential $\Delta\phi_o$ with respect to the ionosphere at the upper end. The local voltage drop is then

equipotential, floating bare tether.

$$\phi_T - \phi_I = \Delta\phi_o - E(L - z) \qquad (2)$$

The electron current collected per unit length when $\phi_T > \phi_I$ is (5):

$$\frac{dI_e}{dz} = e\, n_e d \sqrt{\frac{2e(\phi_T - \phi_I)}{m_e}} \qquad (3)$$

and for the region with $\phi_T < \phi_I$, ions are collected at a rate

$$\frac{dI_i}{dz} = e\, n_e d \sqrt{\frac{2e(\phi_I - \phi_T)}{m_i}} \qquad (4)$$

Here n_e is the ionospheric density, and d is the tether diameter. Ignoring for now the secondary electron emission, we can express the condition of zero net current collection by equating the integrals of (3) and (4) in their respective ranges. This yields the cross-over position as

$$\frac{\ell_c}{L} = \frac{\Delta\phi_c}{EL} = \left(\frac{m_e}{m_i}\right)^{1/3} \tag{5}$$

which is 0.032 for 0^+ ions. Since this is small, we will in what follows ignore the upper positive segment and approximate the potential distribution as

$$\phi_T - \phi_I \cong -E(L-z) \tag{6}$$

The secondary emission of electrons by ion bombardment is characterized by a coefficient γ (electrons per ion) which (except at very low voltages) increases linearly with ion energy [10]:

$$\gamma = \gamma_1(\phi_I - \phi_T) \cong E\gamma_1(L-z) \tag{7}$$

with typical values for γ_1 being 0.1 to 0.2 per KV. We can now multiply $\frac{dI_i}{dz}$ in Eq. (4) times γ and integrate for the total secondary electron current:

$$I_{e,emitted} = \frac{2\gamma_1}{5}\left(\frac{2\,e^3E^3}{m_i}\right)^{1/2} n_e d\, L^{5/2} \tag{8}$$

whereas direct integration of (4) gives a total ion collection of

$$I_M = \frac{2}{3}\left(\frac{2\,e^3E}{m_i}\right)^{1/2} n_e d\, L^{3/2} \tag{9}$$

Comparing (8) and (9), the mean emission coefficient is

$$\bar{\gamma} = \frac{3}{5}\gamma_1 E\, L \tag{10}$$

The vertical distribution of the electron emission is given by

$$\frac{d\left(I_{e,em.}/I_{e,em}(TOTAL)\right)}{d(z/L)} = -\frac{5}{2}\left(1-\frac{z}{L}\right)^{3/2} \tag{11}$$

which indicates a more than linear emphasis on the lower part of the tether, where both, the ion collection rate and the secondary emission coefficient, are greatest.

If we take $\gamma_1 = 0.12$ per KV, E=175 V/Km (an average value for 28°, 300 Km orbits), $n_e = 3\times10^{11}$ m^{-3} (night time level for an average solar activity at 300 Km) and a tether with 2mm diameter, 20 Km length, we calculate from (8) an emitted current of 0.063A.

The electrons are emitted with low energy (a few eV) and then accelerate radially away from the tether under the potential difference $\phi_l - \phi_T$. The electrons are initially uniformly distributed in the azimuthal angle φ about the tether. For a magnetic dip angle I, the pitch angle (ϑ_p) of these electrons will be distributed according to a (normalized) distribution

$$f(\vartheta_p) = \frac{2}{2\pi}\left|\frac{d\varphi}{d\vartheta_p}\right| \quad (12)$$

where the factor of 2 accounts for the fact that both, φ and $-\varphi$ contribute to the same ϑ_p. The relationship is

$$\cos\vartheta_p = \cos I \cos\varphi \quad (13)$$

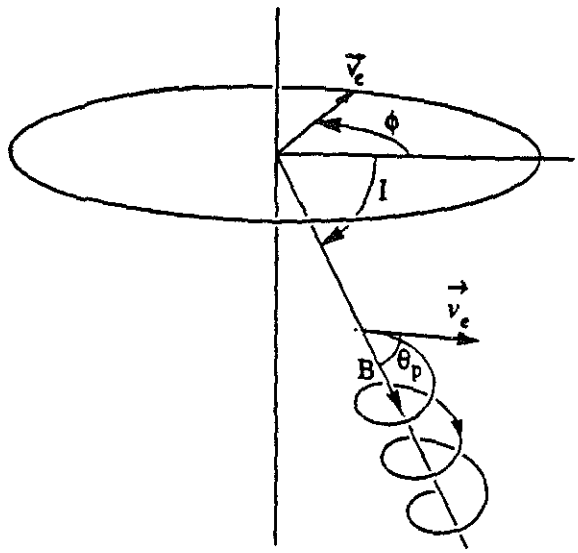

Fig. 3: Geometry of electron emission and pitch determination.

which, when substituted in (12) gives a distribution

$$f(\vartheta_p) = \frac{1}{\pi}\frac{\sin\vartheta_p}{\sqrt{\cos^2 I - \cos^2\vartheta_p}} \quad (14)$$

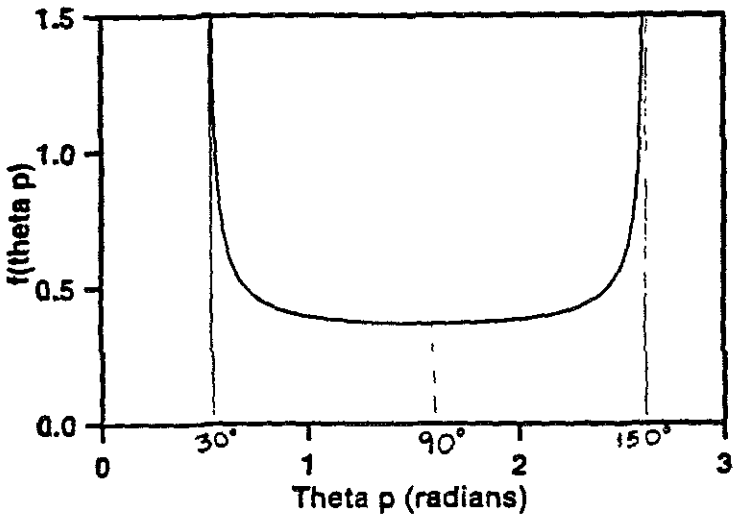

Fig. 4: Electron pitch distribution for a given line). magnetic pitch angle I (rawn for I=30°)

This is shown in Fig. 4, which indicates a fairly wide pitch angle distribution, concentrated about the dip angle I (and $\pi - I$, for the opposite side of the $\vec{B}$ line).

The choice of orbital inclination for the tether has a strong influence on the energy of the injected electrons, and hence on the physics of their interaction with the atmosphere. For a first approximation, the magnetic dipole model is useful. In that model, the horizontal component of the Earth's field is $B_o \sin \vartheta_m$, with $B_o = 3 \times 10^{-5}$ Tesla and ϑ_m being the magnetic co-latitude. Consider an orbit (Fig. 5) inclined i to the geographic equator, (i_m to the magnetic equator), and with its ascending node B at an angle φ_o West of the magnetic pole meridian. At a point P on the orbit, the velocity $\vec{v}$ makes an angle β to the horizontal field $\vec{B}_H$, so that, from Eq. (1),

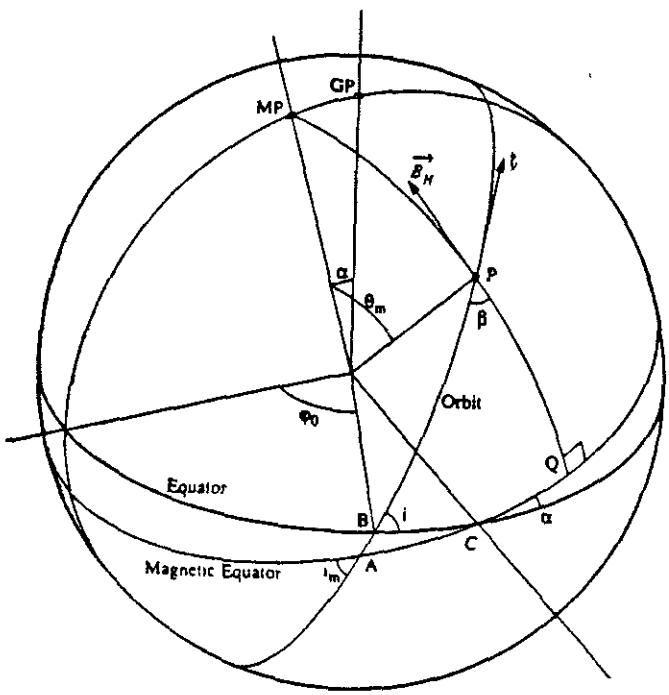

$$E = B_H v \sin\beta = B_o v \sin\vartheta_m \sin\beta \quad (15)$$

Considering the spherical triangle PAQ, where the angle at Q is 90°, we obtain

$$\sin\vartheta_m \sin\beta = \cos i_m \quad (15)$$

and

$$E = B_o v \cos i_m \quad (16)$$

which shows that, to the extent that i_m can be considered constant during one orbit, the induced emf is also constant. The magnetic inclination does vary on a daily basis, however, as φ_o varies. The relationship can be obtained from the spherical triangle ABC:

$$\cos i_m = \cos i \cos\alpha + \sin i \sin\alpha \sin\varphi_o \quad (17)$$

Here the geographic inclination i and the colatitude α of the magnetic pole are indeed constant, and we verify that i_m will fluctuate daily between the limits $|i - \alpha|$ and $i + \alpha$. From (16), then, we obtain an emf centered about

$B_o v \cos i \cos\alpha$, with a superimposed daily oscillation between the limits $B_o v \cos(i+\alpha)$ and $B_o v \cos(i-\alpha)$.

The vertical field component is $-2B_o \cos\vartheta_m$ in this model, so that the dip angle I (Fig. 3) is given by

$$\tan I = \frac{2}{\tan\vartheta_m} \tag{18}$$

with a maximum in each orbit of $(\tan I)_{MAX} = 2\tan i_m$ (at the point nearest the magnetic pole).

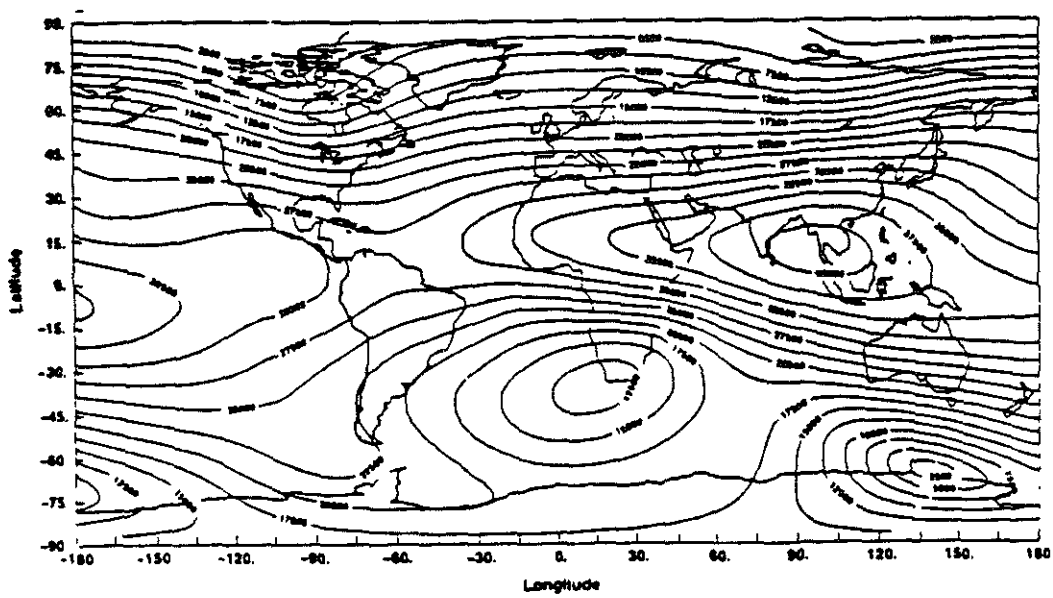

Fig. 6: Contours of constant horizontal field H at the surface of the earthfrom the model IGRF 1980.0.

Besides this simple variation, the irregularities of the actual geomagnetic field manifest themselves more or less strongly, depending on the area being overflown. Especially prominent are the effects of the great negative magnetic anomaly over South Africa, and of the positive Indo-Chinese anomaly (Fig. 6). The former is avoided for orbits with inclination under 15°, whereas the latter will be seen in at least a few orbits per day for any orbital inclination. An example of the complex intra-orbital variations in a 20 Km tether with i=28.5°, z=300 Km (as well as of the underlying daily

oscillation) is shown in Fig. 7, from Ref. [1]. Here the open-circuit voltage fluctuates within some orbits between 1700 and 4500 Volts (E between 85 and 225 V/Km). An interesting observation from Fig. 6 is the relative smoothness of the horizontal field over the mid northern latitudes, where most of the experimentation would be expected to take place. In those areas, the dipole approximation (Eqs. 16, 17, 18) is reasonable.

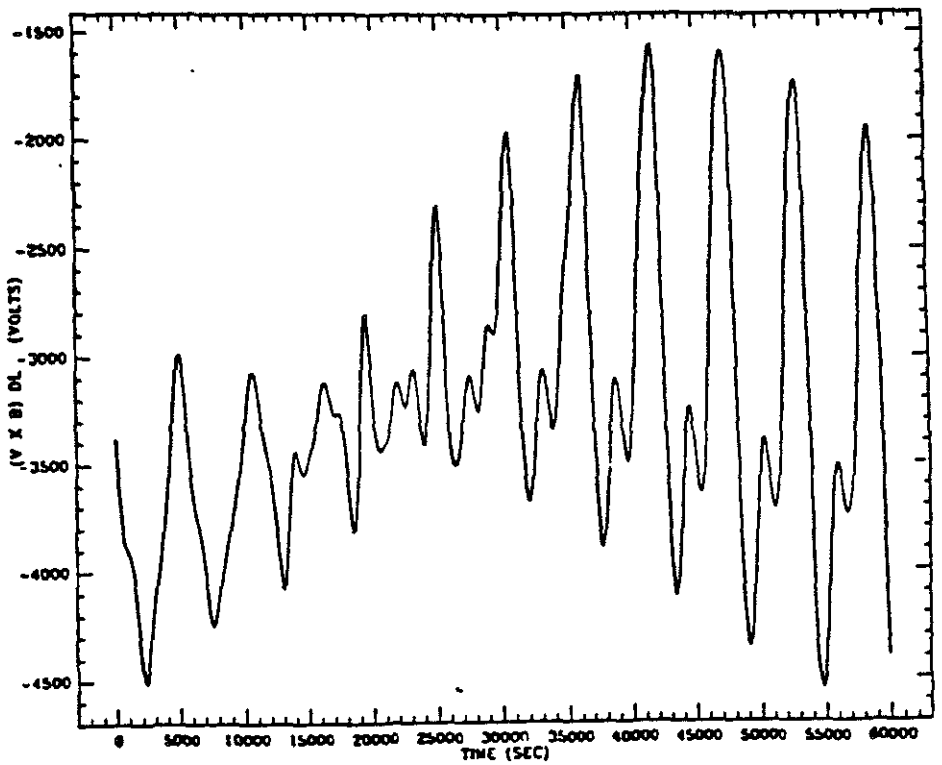

Fig. 7: Open-circuit tether voltage vs. elapsed time (300 Km orbit).

In terms of our scientific objectives, orbits with high inclination tend to be unfavorable because of the associated low induced emf's obtained. For example a sun-synchronous orbit (precessing 360°/yr) at 300 Km altitude has an inclination of 83°, for which i_m varies daily between 72° and 86°. The voltage across a 20 Km tether is then (Eq. 16) between 320V and 1430V, if only the dipole contribution is considered. By contrast, a 45° orbit would give V between 2590V and 3840V, allowing a much stronger electron-atmosphere interaction, and covering most of the range of natural auroral electron energies.

3. Electron-Atmosphere Interactions-Auroral Effects

This section presents a simplified model of the atmospheric slowing down of the extended e-beam formed by the tether-emitted electrons. As will be shown, most of this interaction will occur in the E-layer, between 120 and 150 Km altitude. This region is characterized by a predominance of molecular ions (O_2^+ and NO^+ in particular), which recombine rapidly by dissociation after

sunset. The nighttime ionospheric density is as low as $2\times10^3 cm^{-3}$, while the daytime density is around 10^5 cm^{-3}, with some dependence on the Sunspot cycle. By contrast, the layer where the tether itself will fly (the F layer) is dominated by radiatively recombining O^+ ions (10^5-$10^6 cm^{-3}$) which survive the night with density reduction factors of only 2 to 4.

As electrons with energies in the KV range move in their helical paths down magnetic field lines, they are slowed down by a variety of inelastic interactions with air molecules. The most significant of those interactions is ionization, but for every ionizing event, there are also a number of excitation collisions, followed mainly by prompt photon emission. Because of this, it has been found in many studies [5],[11] that, on average, one ionization is produced for every 35 eV of energy lost by the primary electron. We denote this energy loss per ionizing event as E_i^{eff}, an effective ionization energy. The ionization cross-sections of N_2 and O_2 (summed over all ion states) are quite similar, and can each be approximated for energies above ~30 eV by

$$\sigma_i(\text{Å}^2) \cong 9.72\frac{u-1}{u^2}\ell n\, u \quad ; \; u = \frac{E(eV)}{23.6} \tag{19}$$

Hence, the ionization mean free path is $(n\,\sigma_i)^{-1}$, where n is the total atmospheric density. The E-layer atmosphere can be characterized by a linearly varying scale height; for the mean CIRA reference atmosphere,

$$n(m^{-3}) \cong \frac{1.06\times10^{22}}{(z-95.02)^{3.058}} \qquad \text{(z in Km)} \tag{20}$$

As the primary electrons advance a distance dx in their path, they lose energy by -dE, according to

$$\frac{dE}{dx} = -E_i^{eff} n\,\sigma_i(E) \tag{21}$$

For an electron with a pitch angle ϑ_p about a magnetic line at an angle I to the horizontal, the altitude loss dz is

$$dz = -\sin I \cos\vartheta_p dx \tag{22}$$

We can now rearrange Eqs. (21) and (22) and integrate from an initial energy E_0 at a high altitude ($z \cong \infty$):

$$\int_E^{E_o} \frac{dE}{\sigma_i(E)} = \frac{E_i^{eff}}{\sin I \cos\vartheta_p}\int_z^{\infty} n(z)dz \tag{23}$$

Which can be seen as an equation for the energy E of a primary of pitch ϑ_p at the altitude z. As noted in Sec. 2, electrons are emitted with a pitch distribution $f(\vartheta_p)$ (Eq. 14) which, for one side of the collecting $\vec{B}$ line, goes from $\vartheta_p = I$ (the dip angle) to $\vartheta_p = \pi/2$. Electrons with ϑ_p close to $\vartheta_p = \pi/2$. will lose all their energy at high altitudes, while those with ϑ_p close to I will penetrate most. At any given altitude, Eq. (23) can also be viewed as a relationship between energy and pitch angle. Electrons at that z will have a maximum energy $E_{MAX}(z)$, corresponding to the minimum pitch, I, and a maximum pitch angle ϑ_{pMAX}, for those that have lost almost all their energy above z $\left(E \le E_i^{eff}\right)$. A combination of Eqs. (14) and (23) could be used to derive a primary energy distribution at z, between 0 and $E_{MAX}(z) < E_o$.

However, we are mainly interested here on the integrated ionization rate due to this distribution of primaries, as well as on the resulting population of low-energy secondaries (here "secondaries" refer to electrons from atmospheric ionization; the tether-emitted "secondaries" have become the e-beam "primaries").

The volumetric ionization rate is $n_p v_p n \sigma_i(E)$, where n_p is the density of primaries with speed v_p. Since different pitch angles correspond at a given height to different energies, we select the differential flux $d(n_p v_p)$ corresponding to a pitch interval $(\vartheta_p, \vartheta_p + d\vartheta_p)$. Ignoring the spreading of the beam, this is taken to be the fraction $f(\vartheta_p)d\vartheta_p$ (Eq. (14)) of the flux emitted by the tether at the origin of the magnetic tube connecting to the point being considered. The width of the e-beam perpendicular to the tether is taken to be $2r_L$, the Larmor diameter at the tether, so that, before absorption, the flux (two-sided) is

$$\Phi_o = \frac{1}{2r_L \cos I\, e} \frac{dI_{e.em}}{dz} \tag{24}$$

and so $d(n_p v_p) = \Phi_o f(\vartheta_p) d\vartheta_p$, giving for the ionization rate at some altitude z

$$\dot{n}_s(z) = n(z)\Phi_o \int_I^{\vartheta_{pMAX}} \sigma_i[E(\vartheta_p)] f(\vartheta_p) d\vartheta_p \tag{25}$$

Note here that the upper limit ϑ_{pMAX} is less than the original $\frac{\pi}{2}$, due to the loss above the current z level of the high-pitch primaries.

In the steady state, the secondary electron population would be determined by the balance between N_2 and O_2 ionization, and the dissociative recombination of O_2^+ and NO^+ (since N_2^+ converts rapidly [11] via $N_2^+ + O \rightarrow NO^+ + N$). Assuming a similar recombination cross-section σ_{rec} for both ions, and charge neutrality, with negligible background ion contribution, this would yield

$$n_s(z)_{ss} = \sqrt{\frac{\dot{n}_s(z)}{\bar{c}_s \sigma_{rec}(E_s)}} \tag{26}$$

where $\bar{c}_s$ is the mean thermal velocity for secondary (ionization produced) electrons of energy E_S (~0.3 eV). However, the buildup time of this population is of the order of $(n_s)_{ss} / \dot{n}_s$; using $\dot{n}_s \sim 10^3$-10^4 $cm^{-3}sec^{-1}$ and $(n_s)_{ss} \sim 10^5 cm^{-3}$ (to be shown shortly), this time is 10-100 sec, much longer than the roughly 1 msec dwell time of the 10 m wide beam moving at 8 km/sec. Thus, the plasma density remains almost unaltered at its background level; on the other hand, the 1 msec illumination time is long enough to produce a quasi-steady ionization rate $\dot{n}_s$ (Eq. 23), with its associated excitation and prompt emission effects.

As an example of application for conditions of interest to our experiment, consider emission from near the lower end of a 20 Km tether, with a local bias of 3000V (E_0=3000V) at a location where the magnetic dip angle is I=45°. We use our Sec. 2 estimate of a total emitted electron current of 0.063 Amp, and, from Eq. (11), a local lengthwise emission rate $\left|\frac{dI_{em}}{dz}\right| \cong \frac{5}{2}\frac{0.063}{20{,}000} = 7.88 \times 10^{-6} A/m$. For an approximate value r_L=5m, the high-altitude flux (Eq. 24) is then $\Phi_o = 6.97 \times 10^{12} m^{-2} sec^{-1}$.

The results of Eqs. (25), (26) for this case are summarized in Fig. 8. Notice, first of all, that absorption is complete at approximately z=120 Km. The rapid increase of $(n_s)_{ss}$ and $\dot{n}_s$ near this level is probably a result of oversimplifications in the model, which ignores the many low-energy reactions occurring there.

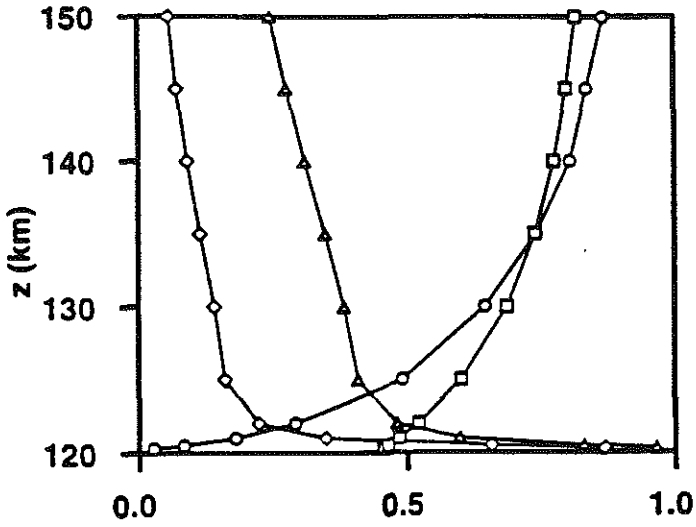

Fig. 8: Vertical distribution of steady state induced plasma density $\left(n_e / \left(7\times10^5 cm^{-3}\right)\right.$ —▲— $\left.\right)$, ionization rate $\left(\dot{n}_e / 2\times10^4 cm^{-3}\sec^{-1}\right.$ —◇— $\left.\right)$ maximum pitch angle, $\left(\vartheta_{pMAX} / 100^\circ\right.$ —□— $\left.\right)$ and maximum primary electron energy $\left(E_{MAX} / 3000eV\right.$ —○— $\left.\right)$. Here $E_o 3000eV$ and $dI_{em} / dz = 7.88\times10^{-6} A / m$.

The ionization rates indicated in Fig. 8 range from a few thousand to a peak of about 15,000 per cm^3, per sec. For comparison to natural auroras, note that the incoming energy flux is basically 1/2 of the flux Φ_o, times E_O $(\frac{1}{2}\times6.97\times10^{12}\times1.6\times10^{-19}\times3000 = 1.67\times10^{-3}\frac{W}{m^2}$, or 1.67 erg/$cm^2$/sec). Natural ionization rates in $cm^{-3}sec^{-1}$ are frequently quoted as about 3000 times this flux, in erg/cm^2/sec, which would imply 4000 $cm^{-3}sec^{-1}$ in our case. This is indeed close to the average $\dot{n}_e$ in the main absorbing layer (Fig. 8).

Incidentally, this energy deposition rate (1.67 erg/cm^2/sec) is intermediate between those for Types I and II of natural aurora for which type I is the weakest visually observable type. In consistency with this, notice also in Fig. 8 that the steady state ionization $(n_e)_{ss}$ would be of the order of $3\times10^5 cm^{-3}$, much greater than the natural nighttime plasma density, and even larger than most daytime values.

As a second example, Fig. 9 shows results for the same tether, but from a point about halfway down its length, where E_O=1500V and the emission rate is reduced by a factor $(0.5)^{3/2}$=0.35 compared to the tip value. The absorption is shifted upwards by about 20 Km, and the ionization rate is reduced to the

range about 300 $cm^{-3}sec^{-1}$. The energy flux is now lower by $(0.5)^{5/2}=0.18$, or 0.30 $erg/cm^2/sec$, about one half that for Type I auroras.

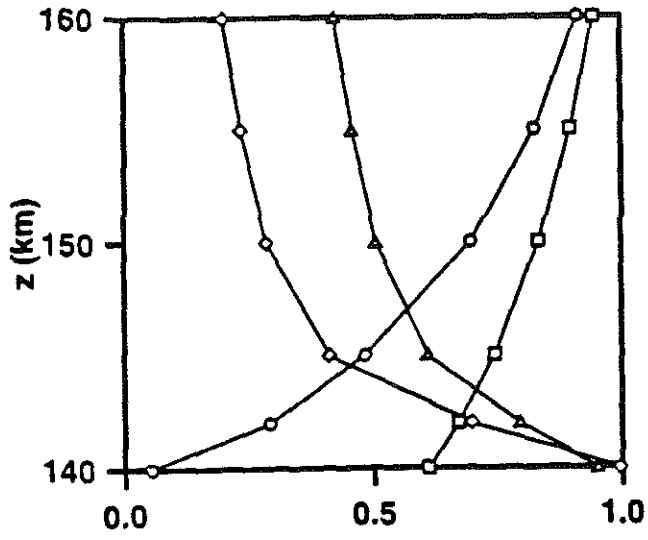

Fig. 9: Similar to Fig. 8, but for E_o=1500V, $dI_{em}/dz=2.79\times10^{-6}$ A/m. The scales are:

$n_s / 1.6\times10^5 cm^{-3}$
$\dot{n}_s / 900 cm^{-3}\sec^{-1}$
$\vartheta_{pMAX} / 75^\circ$
$E_{MAX} / 1100 eV$

Exploratory calculations indicate that the effect of a lower dip angle I (but with the same E_o and emission rate) is not very strong. For I=30°, the ionization rate is about 1/4 that for 45°, and occurs about 2 Km higher.

4. Observational Considerations

We begin this section with a review of the quantities that need to be measured for a quantitative experiment, and of the most likely instrumentation for the purpose.

Knowledge of the primary electron flux can be obtained from a combination of differential current readings at points along the tether, and a careful pre-flight calibration of the emission coefficient γ vs. ion energy for the material used. Direct magnetic perturbation measurements could also be performed, but it would be difficult to separate the emitted electron currents away from the tether from the basic wave-carried currents implied by the ion collection in the lower part of the tether and the electron collection in its upper part.

Observation of the visible or IR emissions from the excited E-layer are likely to yield the most detailed picture of events. Two observation geometries can be used: (a) From the ground, with the advantage of allowing vertical resolution (Fig. 10), and (b) From the spacecraft, looking down $\bar{B}$ lines, with the advantage of allowing longer observations, and hence finer spectral resolution. An interesting, but more technically demanding alternative, would be to use an on observing sould satellite, leading or lagging the tether carrier by ~100-200Km in the same orbit.

Considering the observational geometry of Fig. 10, the number of photons received at the detector per second from the layer Δz would be

$$\Phi_D = \dot{n}_{em}\Delta z \frac{d}{\cos\alpha} \frac{L}{\tan I} \frac{A_D}{4\pi(z/\sin\alpha)^2} \qquad (27)$$

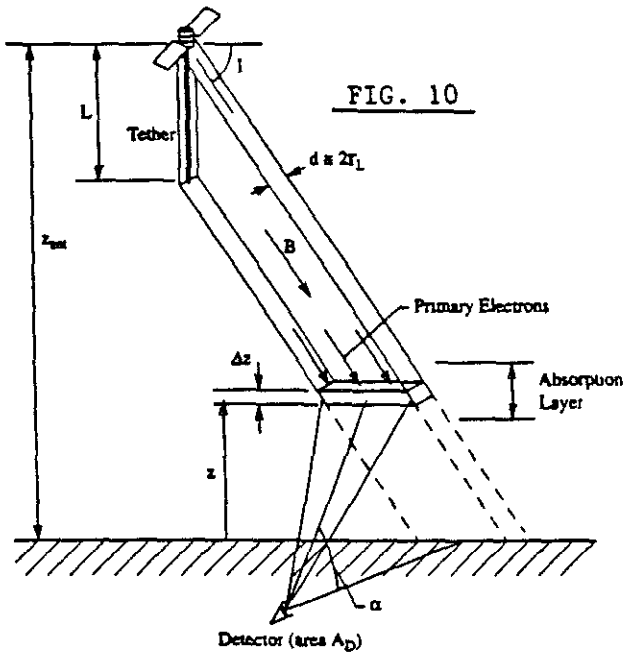

FIG. 10

where $\dot{n}_{em}$ is the volumetric emission rate of photons of the type considered. The book by A. Jones [5] discusses production rates of radiating species for natural auroras. A standard observed emission is that of the nitrogen ion line $N_2^+(4278\text{Å})$. For this line, Jones (Ref. [5]), Fig. 4.24) shows a peak emission rate of about 70 $cm^{-3}sec^{-1}$ per $erg/sec/cm^2$ primary flux, which is in the range expected in our case. If we wish to resolve $\Delta z = 1Km$, with d=10m, $\alpha = 45°$, I=45°, L=10 Km (say, the lower 10 of a 20 Km tether), A_D=100cm^2 and z=125 Km, we obtain from Eq. (27) a photon flux of 250/sec for this line. A second standard for observation is the atomic oxygen line O(^{1}S) 5577 Å, with about four times the yield of N_2^+4278, and the total photon count from known observable transitions is about 50 times that for N_2^+4278.

In order to examine the detector feasibility, we introduce, following [5] the Rayleigh as a unit of source luminosity ($\frac{4\pi}{10^6}$ times the no. of photons per cm^2, per sr., per second at the detector). With this definition, Eq. (27) yields a luminosity in Rayleighs of

$$B = \frac{1}{10^6} \dot{n}_{em} \left(\frac{d}{\cos \alpha} \right) \tag{28}$$

with cgs units for $\dot{n}_{em}$ and d. For the N_2^+4278 line and the other conditions of our example, we find B=0.1R. For reference, natural auroras yield about 100R per erg/cm^2/sec energy flux; the discrepancy is due to the small depth (~10m) of the emitting layer in the direction of observation, compared to the usual ~10 Km for natural auroras.

For a detector with a count rate per Rayleigh e_1, observing a single line for a time t yields a signal count e_1Bt, and a total count rate, including a dark count rate i_D, of $(e_1B+i_D)t$. Since the fluctuations are the square root of the total count, this yields a signal/noise ratio

$$s/N = \sqrt{\frac{e_1 B t}{1 + (i_D / e_1 B)}} \tag{29}$$

A Fabry-Perot spectrometer can yield $e_1 \cong 10^4$ per R. For the geometry of Fig. 9, we may track and obtain useful data for about 3 sec. With a medium dark rate of i_D=100 sec^{-1}, we calculate S/N=52, which is adequate. On the other hand, a grating spectroscope will be limited to e_1~100 counts/R, and if we attempt to observe, say, 10 lines, the time per line is 1/10 of total, which yields S/N=0.5, showing inadequate resolution.

The S/N situation is much improved for observation from the spacecraft, where B can indeed be of the order of 10-100 Rayleighs, although vertical resolution must then be given up (except if a second observing satellite is used).

We conclude with some considerations about orbit selection. For ease of optical observation from the ground, we would like to assure repeated overflights of selected ground stations. This can be accomplished by placing the tether-carrying spacecraft at an altitude which yields an integer number of orbits per day. Two convenient choices are z_{SAT}=279 Km (16 orbits/day) and 572 Km (15 orbits/day). The latter choice would actually produce two overflights per day of a given spot on the ground, one on the northbound and one on the southbound parts of the orbit. The orbital inclination is not a critical factor, except, as noted in Sec. 2, for the near-polar orbits, which would yield too low voltages. In order to obtain good coverage of the mid-latitudes, where natural auroras do not occur, inclinations from 20° to 60° seem appropriate.

Nighttime observation would have advantages, in that any competing effects of the natural ionospheric background would be minimized, as would stray light in optical detectors. Pulsing the end contactors of the tether on/off at some high rate would also be a useful technique for phase-locked detection.

5. Conclusions

Significant localized enhancements of the ionspheric emissions rates appear possible from the topside bombardment of the E-layer by secondary electrons liberated by the ions falling on a floating bare tether of some 20 Km length. Observation of the transient increased emitted light appears feasible, although challenging, and would, if correlated with the incident electron beam characteristics, yield important information on auroral processes.

APPENDIX. Tether Lifetime Estimates

Destruction by a hypervelocity impact is probably not a critical issue becasue the danger decreases rapidly with increasing tether diameter. For a (low) 279 km orbit, the space debris flux may be neglected against the flux of meteoroids, which is only weakly dependent on altitude. A 2 mm thick, 20 km long tether, if made of aluminum, would take about 3 severing hits per year (Figure 11 in Ref. 12), yielding a 4-month mean lifetime for our tether. In contrast, the severing rate of a 0.75mm diameter, as in SEDS 2, would be 10 times larger, leading to a 12 days lifetime (SEDS 2, which was actually made of Spectra 1000, was cut after 5 days; on the other hand, the remaining 8 km length was finally brought down by air drag at twice its lifetime - 30 days - for meteoroid severing).

Altitude loss due to magnetic drag is, on the contrary, critical. For $E = 175V/km$ and $n_e = 3\times10^{11}m^{-3}$, the total ion current I_M (ignoring electron emission), as given by (9), is about 0.25A, and the average current is 3/5 of this value. Accross the full *emf* of $3.5kV$, this current represents an orbital power loss of 525 watt. If this loss is left unbalanced, the time to drop 10 Km from the 279 km orbit would roughly be

$$\frac{10km}{6620km}\frac{\frac{1}{2}(8km/s)^2 M}{525w} \equiv 1.1M \text{ (tons) days,}$$

where M is the joint mass of spacecraft and tether system.

Consider finally the dynamical equilibrium of the tether under the magnetic and gravity-gradient forces. Such equilibria have proved generally unstable in the case of insulated tethers. Because our current is weak, we find here that the tether is nearly straight and vertical at equilibrium, and that this is very weakly unstable.

The equations describing motion of a mass m at tether bottom, in the orbital plane, are [13]

$$r\left(\ddot{\theta}+3\sin\theta\cos\theta\right)+2\dot{r}\left(1+\dot{\theta}\right)=\frac{T\sin(\theta-\alpha_o)}{m\omega^2} \tag{A1}$$

$$\ddot{r}-r\left(\dot{\theta}^2+2\dot{\theta}+3\cos^2\theta\right)=-\frac{T\cos(\theta-\alpha_o)}{m\omega^2} \tag{A2}$$

where $r(\tau)$ and $\theta(\tau)$ are polar coordinates for m, $T(r)$ is tension, $\tan\alpha_o(\tau)$ is tether slope at the end mass, relative to the vertical, and τ is the

dimensionless time ωt $(2\pi/\omega \equiv$ orbital period) (Fig. A1). For a massless, inextensible tether, the equation determining the local slope tan $\alpha(\tau,\tilde{s})$ is [13]

$$\frac{\partial\alpha}{\partial\tilde{s}} = \frac{LI_iB}{T} \tag{A3}$$

where $s \equiv \tilde{s}L$ is tether arc-length, with $\tilde{s}=0$ at the end mass, $\tilde{s}=1$ at the spacecraft, and $\alpha_o \equiv \alpha(\tau,0)$; for simplicity we took B normal to the orbital plane. For the bare tether I_i is $\tilde{s}$ – dependent (T is not), Eq. (4) taking here the form

$$\frac{\partial I_i(\tau,\tilde{s})}{\partial\tilde{s}} = Len_e d\sqrt{\frac{2eE(L-z)}{m_i}} \tag{A4}$$

with $z=L$ at $\tilde{s}=1$, and

$$\frac{\partial(z/L)}{\partial\tilde{s}} = \cos\alpha \tag{A5}$$

Equations (A3-A5) yield

$$\frac{\partial^2\alpha}{\partial\tilde{s}^2}\frac{\partial^3\alpha}{\partial\tilde{s}^3} = -\frac{9}{8}\left(\frac{LI_MB}{T}\right)^2\cos\alpha,$$

$$\frac{\partial^2\alpha}{\partial\tilde{s}^2} = 0 \quad \text{at} \quad \tilde{s}=1,$$

$$\frac{\partial\alpha}{\partial\tilde{s}} = 0 \quad \text{and} \quad \alpha=\alpha_o \quad \text{at} \quad \tilde{s}=0.$$

The solution for $\alpha(\tau,\tilde{s})$ clearly allows relating $r(\tau),\theta(\tau)$ to $\alpha_o(\tau),T(\tau)$; for small LI_MB/T we find

$$\theta-\alpha_o \cong \frac{3}{14}\frac{LI_MB}{T} + 0\left[\left(\frac{LI_MB}{T}\right)^3\right], \tag{A6}$$

$$r/L \cong 1-\frac{59}{49\times72}\left(\frac{LI_MB}{T}\right)^2 + 0\left[\left(\frac{LI_MB}{T}\right)^4\right] \tag{A7}$$

Equations (A1), (A2), (A6) and (A7) finally determine α_o, T, θ and r as functions of τ. At equilibrium,

$$\alpha_o = 0, \quad \theta = \frac{5}{14}\alpha(\tilde{s}=1) \cong \frac{1}{14}\frac{I_M B}{m\omega^2},$$

$$T \cong 3m\omega^2 L\left[1 - 4.5\times 10^{-3}\left(\frac{I_M B}{m\omega^2}\right)^2\right],$$

$$r/L \cong 1 - 1.9\times 10^{-3}\left(\frac{I_M B}{m\omega^2}\right)^2.$$

Note that $LI_M B/T = I_M B/3m\omega^2 \cong 1.2kg/m$ for $I_M = 0.25A$ and $B = 0.2$ Gauss. When the system is linearized at equilibrium, the resulting eigenvalues have imaginary parts

$$\lambda_1 \cong \pm\sqrt{3}, \qquad \lambda_2 \cong \pm 1.2\times 10^3 \frac{m\omega^2}{I_M B'}$$

the first two having positive real parts of order $\left(I_M B/m\omega^2\right)^3$, leading to growth times of order of 1 year.

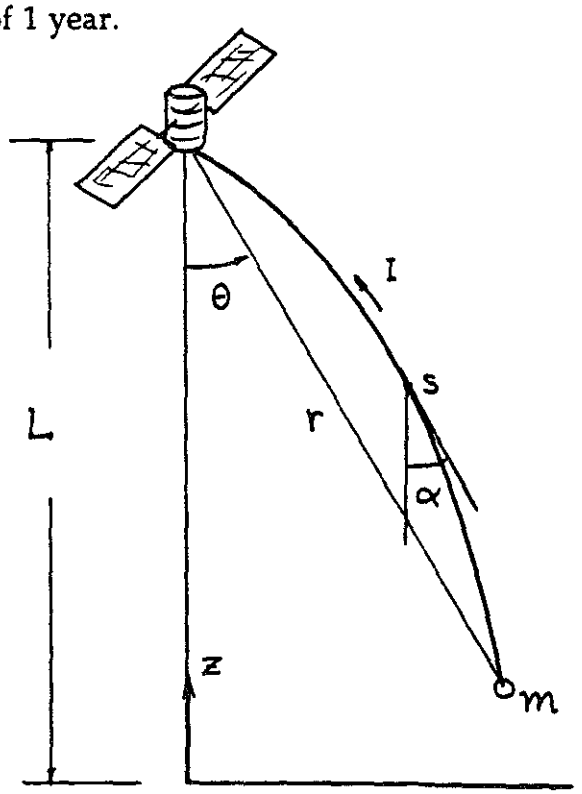

Fig. 1: Geometry for tether deformation

REFERENCES

(1) M. Martinez-Sanchez and D.E. Hastings, "A Systems Study of a 100 KW Electrodynamic Tether". The Jl. of Astronautical Sciences, Vol. 35, 1987, pp. 75-96.

(2) Wilbur, P. and Laupa, T., "Plasma Contactor Design for Electrodynamic Tether Applications". Adv. in Space Res., Vol. 8, 1988, pp. 221-224.

(3) Gerver, M.J., Hastings, D.E., and Oberhardt, M., "Theory of Plasma Contactors in Ground-Based Experiments and in Low Earth Orbit". J. of Spacecraft, Vol. 27, 1990, pp. 391-402.

(4) Sanmartin, J.R., Martinez-Sanchez, M. and Ahedo, E., "Bare Wire Anodes for Electrodynamic Tethers". J. of Propulsion and Power, Vol. 9, No. 3, May-June 1993, pp. 353-360.

(5) Jones, A.V., Aurora, D. Reidel Publ. Co., 1974.

(6) Kelley, M.C. The Earth's Ionosphere, Academic Press, 1989.

(7) Lysak, R.L., Auroral Plasma Dynamics. American Geophysical Union, Geophysical Monograph 80 (1993).

(8) Lee, E.T.P., Bien, F., Anheiser, M. Lyons, R., Kolb, Ch. and O'Neill, R.R. EXCEDE: Spectral, Final Report, AFGL-TR-85-0125, Air Force Geophysics Lab, Bedford, MA 1985.

(9) Paulsen, D.E., Ratkowski, A.J., Bien, F., Howlett, L.C., Thurgood, I.L., Kofsky, I.L., Boquist, W., and Murphy, R.E., EXCEDE III-Atmospheric Excitation by Electron Deposition, Eos Trans. AGU, 71, 1500 (1990).

(10) Cobine (J.D.) Gaseous Conductors, Chapter V, Dover, 1958.

(11) Martinez-Sanchez, M., Cheng, W.K., Dvore, D. and Zahneiser, M., "Electron Energy Distribution from Intense Electron Beams in the Upper Mesophere and Lower Thermosphere". J. of Geophys. Res., Vol. 97, No. A2, pp. 1363-1375, Feb. 1, 1992.

(12) Flury, W., and Klindrad, H. "The Space Debris and Meteoroid Hazard for Orbiting Tethers", in Proc. Int. Roundtable on Tethers in Space, ESA, WPP-081, 1994, pp. 528-546.

(13) Beletsky, V.V. and Levin, E.M., Dynamics of Space Tether Systems, Ch. 5, Adr. in the Astronautical Sciences, Vol. 83, (1993).